

Reentrant phase transitions in threshold driven contagion on multiplex networks

Samuel Unicomb,¹ Gerardo Iñiguez,^{2,3,4} János Kertész,² and Márton Karsai^{1,*}

¹*Université de Lyon, ENS de Lyon, INRIA,
CNRS, UMR 5668, IXXI, 69364 Lyon, France*

²*Department of Network and Data Science, Central European University, H-1051 Budapest, Hungary*

³*Department of Computer Science, Aalto University School of Science, 00076 Aalto, Finland*

⁴*IIMAS, Universidad Nacional Autónoma de México, 01000 Ciudad de México, Mexico*

Models of threshold driven contagion successfully explain the cascading spread of information, behaviour, systematic risks and epidemics on social, financial and biological networks. Contradicting real observations, on single-layer networks with sufficiently high connectivity such models predict no global cascades. We investigate threshold driven contagion on weight heterogeneous multiplex networks and show that they remain susceptible to global cascades at any level of connectivity; and with increasing edge density pass through alternating phases of stability and instability in the form of reentrant phase transitions of contagion. Our results provide a missing theoretical explanation for the observation of large scale contagion in highly connected but heterogeneous networks.

INTRODUCTION

Information-communication technology has radically changed human social and economic interactions [1] by introducing new means of transmitting ideas, behaviour, and innovation [2, 3], pushing farther the limitations in complexity caused by cognitive and time constraints [4, 5]. New technology provides an increasingly accurate picture of human interactions, allowing a detailed mapping of the underlying network structures that mediate, e.g., epidemic processes [6, 7]. In complex contagion [3], characteristic for spreading of innovations, rumors or systemic risk, transmission is a collective phenomenon where all social ties of an individual may be involved. Consequently, degrees (number of links) of nodes are critical to the final dynamical outcome of spreading [8]. Relative influence from a large fraction of neighbors is easier to achieve in a small egocentric network compared to individuals with many acquaintances. This behaviour is well captured by threshold models of social contagion on single-layer networks, which predict large-scale cascades of adoption only for relatively sparse networks [8–11]. Empirical social networks, however, indicate that individuals can maintain hundreds of ties [5, 12], with strength of interaction varying across a range of social contexts [13–15]. These systems constitute dense and strongly heterogeneous networks that nonetheless exhibit frequent system-wide cascades of social contagion [16–20].

We address this issue by incorporating some of the most relevant features of empirical social networks into a conventional threshold model. First, we consider that network ties are heterogeneous and can be characterized by edge “types”. In the case of social networks, these edge types vary in “quality” [21, 22], usually associated with the intimacy or perceived importance of the relationship by the interacting individuals [23, 24], which arguably scales with the strength of interpersonal influence [25, 26]. Heterogeneity in tie quality and influence are well modeled by multiplex structures, as has been recognized in both network science [27, 28] and social science [29, 30], particularly with respect to social contagion [31–34]. In multiplex models of social networks, individual layers represent the social context of a relationship (e.g. kinship, acquaintance). Multiplexity allows us to classify ties by their social closeness, as recognized by Dunbar’s intimacy circle theory [23]. According to this theory, due to cognitive and time resources being finite but necessary to maintain social ties, individuals actively care about a limited number of relationships, and organize them into intimacy circles that increase in size as they decrease in importance [35, 36]. Ego networks are thus comprised of a small but high-strength circle of intimate relationships, like family and close friends, followed by larger but lower-strength circles of distant friends and acquaintances. Empirical

* marton.karsai@ens-lyon.fr

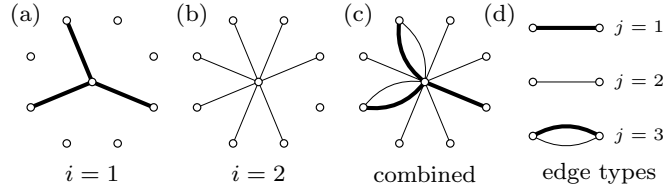


FIG. 1. (a-b) Egocentric view of multiplex structure with $M = 2$ layers, where edge density increases ($\delta_z > 1$) and edge weight decreases ($\delta_w < 1$) in each layer i . (c) Egocentric network overlap between layers. (d) Emergent composite edge types in the overlapping network. In the multiplex, the central node has degree vector $\mathbf{k} = (1, 5, 2)^T$, encoding layer overlap.

evidence for intimacy circles includes the heterogeneous distribution of dyadic social commitments (number of interactions or time devoted to peers) commonly observed in social networks [37, 38]. Strikingly, this inverse relation between the cost of maintaining a certain edge type, and the abundance of that edge type, can be seen as an entropy maximization process [39] that applies to any system with heterogeneous cost of edge formation and finite node resources. As such, although we use the language of social networks, our results are of relevance to other systems, e.g. financial [40–42] and biological [6, 7] contagion.

Here we study threshold driven contagion over such heterogeneous multiplex networks organized hierarchically. By means of analytical and numerical tools, we show that multiplexity can lead to global cascades in networks with average degree in the hundreds or thousands, perturbed only by a single initial adoption. As a novel observation, we also show that in a multiplex network with increasing link density a sequence of phase transitions occur, resulting in alternating phases of stability and instability to global cascades.

RESULTS

Our model builds upon previous studies of threshold driven processes [8–11] and multiplex networks [27, 28]. We define contagion as a binary-state dynamics over a weighted, undirected multiplex network of N nodes connected throughout M layers (Fig. 1). A node represents an individual u present in every layer, with layers being the social contexts in which individuals interact. In each layer i ($1 \leq i \leq M$), the degree of node u (number of relationships in a given context) takes discrete values $k_i(u) = 0, \dots, N - 1$ according to the degree distribution $P_i(k)$. The edge weight $w_i(u, v)$ captures the quality of an edge, i.e. the intimacy level of a social tie and thus the total capacity of nodes u and v to influence each other via layer i . The network allows for layer overlap [43] as the same nodes may be connected in multiple layers, like individuals who share several social contexts (Fig. 1c). We consider a simplified multiplex structure by assuming that: (a) edges in the same layer have identical weight [$w_i(u, v) = w_i$]; (b) degrees of a node in different layers are independent; and (c) the degree distribution $P_i(k)$ has identical functional form in each layer, differing only in the average degree $z_i = \sum_k k P_i(k)$. In order to reproduce the hierarchical organization of edges suggested by intimacy circle theory [35, 36], we assume that the interaction strength w_i and average degree z_i scale linearly with the layer index i ,

$$w_{i+1} = \delta_w w_i \quad \text{and} \quad z_{i+1} = \delta_z z_i, \quad (1)$$

with $\delta_w \leq 1$ and $\delta_z \geq 1$. In other words, ego networks are comprised of a small number of high-cost neighbors strongly influencing the ego (Fig. 1a), and a larger number of low-cost neighbors weakly influencing the ego (Fig. 1b). With Eq. (19), the distributions of weights and densities by layer are prescribed by four free parameters ($w_1, \delta_w, z_1, \delta_z$). Finally, the average degree of the multiplex network is $z = z_1(\delta_z^M - 1)/(\delta_z - 1)$.

In a binary-state model of contagion, nodes are in one of two mutually exclusive states, susceptible or infected (also called adopter or activated in the social contagion literature). At the same time, since nodes must be either connected or disconnected in each of the M network layers, their interaction is characterized by one of 2^M composite edge types (Fig. 1d). We index these types by j (disregarding nodes disconnected

TABLE I. Possible extensions of the Watts threshold rule to multiplex networks. Node state may be determined by individual layer thresholds ϕ_i and neighbor configurations (k_i, m_i) , or by a single threshold ϕ and a weighted sum over the local neighborhood (\mathbf{k}, \mathbf{m}) . The latter is a special case and the focus of this paper, where the network can be projected to a weighted network without loss of information relevant to the dynamics.

multiplex <i>and</i>	multiplex <i>or</i>	weighted multiplex
$m_i \geq \phi_i k_i \quad \forall i$	$\exists i \text{ s.t. } m_i \geq \phi_i k_i$	$\mathbf{m} \cdot \mathbf{w} \geq \phi \mathbf{k} \cdot \mathbf{w}$

in all layers), so that $1 \leq j \leq 2^M - 1$. The configuration of a node is thus described by the number of neighbors k_j and infected neighbors m_j across edges of type j , with $0 \leq m_j \leq k_j$. We store k_j and m_j in the degree vector \mathbf{k} and partial degree vector \mathbf{m} , respectively, each having dimension $2^M - 1$. We also use \mathbf{w} to store the sum w_j of weights of layers comprising the composite edge of type j . In terms of indexing note that consistently i indicates different layers, while j assigns different composite edge types.

The threshold rule proposed by Watts [8–11] defines the fraction ϕ of neighbors that must be infected for an ego to adopt. This rule can be extended to multiplex networks in several ways (Table I). One may argue that the activation of a node is determined by individual layer thresholds ϕ_i and neighbor configurations (k_i, m_i) . That is, a node becomes active when $m_i \geq \phi_i k_i$ in every layer (termed the multiplex *and* rule by Lee [33]), or in at least one layer (multiplex *or* rule [33]). In these cases, the dynamics of complex contagion is unresponsive to changes in weight heterogeneity between layers (Fig. 2), and requires a node to consider separately M bits of information (the result of the threshold rule in each layer) upon updating state. We instead argue that in real systems, individuals do not explicitly consider layer structure in decision making and perceive influence in aggregate, reminiscent of systems like neural networks [44, 45]. We suggest that node state is determined by a single threshold ϕ and a weighted sum of influence over its local neighborhood (\mathbf{k}, \mathbf{m}) , such that a node becomes infected when $\mathbf{m} \cdot \mathbf{w} \geq \phi \mathbf{k} \cdot \mathbf{w}$ (weighted multiplex rule). Note that the multiplex *and* and *or* rules work as upper and lower bounds on the speed of contagion under the weighted multiplex rule (Fig. 2a and b). Our model and analytic framework allow for a rate p of spontaneous adoption, which may be used to incorporate the effect of influence external to the network [10, 14, 16, 46].

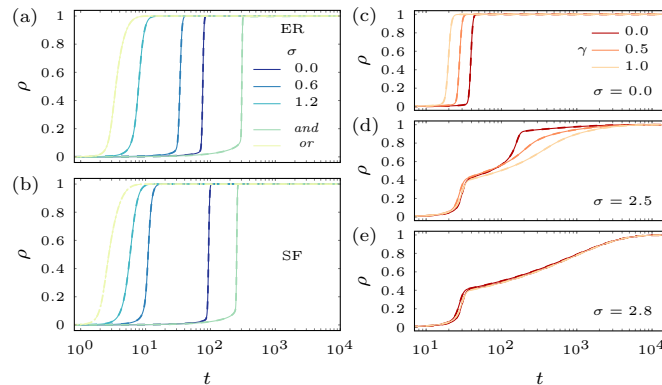


FIG. 2. Density $\rho(t)$ of infected nodes at time t for $M = 2$ layer networks. (a-b) Accelerative effect of increasing weight standard deviation σ in Erdős-Rényi (ER) and scale-free (SF) configuration-model duplexes, with relative density $\delta_z = 2$ and threshold $\phi = 0.18$. The multiplex *and* and *or* threshold rules can be viewed as upper and lower bounds, respectively, on spreading time. Layer thresholds are $\phi_i = 0.18$ for $i = 1, 2$. (c-e) Diminishing effect of layer overlap γ when increasing weight standard deviation σ in an ER duplex with $\delta_z = 10$ and $\phi = 0.15$. Simulations (solid lines) are averaged over 10^3 realizations of a network of $N = 10^5$ nodes and average degree $z = 10$. Rate of spontaneous adoption is $p = 2 \times 10^{-4}$. AME solutions (dashed lines) are indistinguishable from numerical simulations for all definitions of the threshold rule.

We use the approximate master equation (AME) formalism [47, 48] to explore our model analytically. Similar to earlier solutions [10, 14, 16], at any time t , the average density of infected nodes $\rho(t)$ and the average probability $\nu_j(t)$ that a j -type neighbor of a susceptible node is infected are governed by the system

of coupled differential equations:

$$\begin{aligned}\dot{\nu}_j &= g_j(\boldsymbol{\nu}, t) - \nu_j, \\ \dot{\rho} &= h(\boldsymbol{\nu}, t) - \rho,\end{aligned}\tag{2}$$

where $g_j(\boldsymbol{\nu}, t)$ and $h(\boldsymbol{\nu}, t)$ are known functions (see Supplementary Information [SI] and [14]). A numerical solution of Eq. (2) reveals the dynamical evolution of threshold driven contagion on our model (Fig. 2). A linear stability analysis [49] shows the effect of single node perturbations in the multiplex and provides boundaries in the phase diagram (see dashed lines in Fig. 3 for the weighted threshold rule, and SI for the multiplex *or* rule). We derive a global cascade condition via the Jacobian matrix J corresponding to Eq. (2), evaluated at the fixed point $\boldsymbol{\nu}^* = \mathbf{0}$,

$$J_{ij}^* = -\delta_{ij} + \left. \frac{\partial g_i(\boldsymbol{\nu})}{\partial \nu_j} \right|_{\boldsymbol{\nu}=\boldsymbol{\nu}^*},\tag{3}$$

which has eigenvalues λ_i . System-wide cascades of contagion occur if $\text{Re}(\lambda_i) > 0$ for any i .

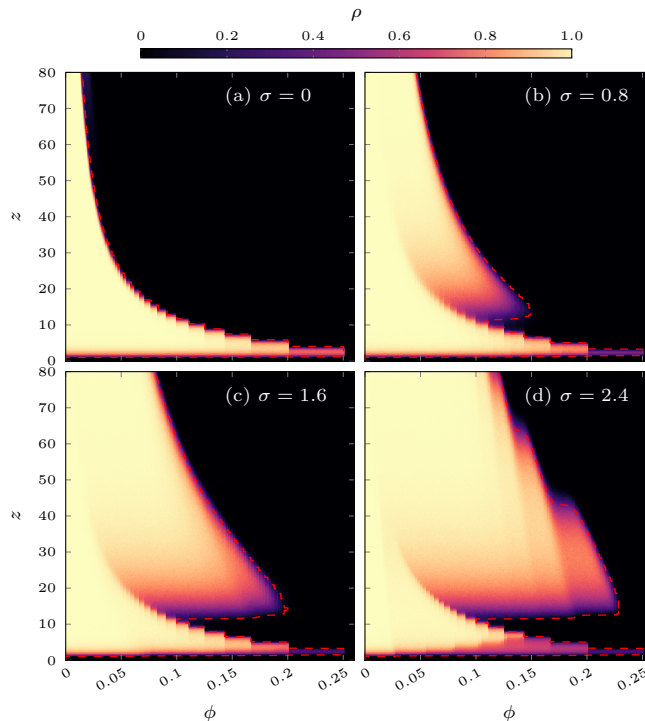


FIG. 3. (a-d) Expected final cascade size $\rho(\infty)$ with increasing weight heterogeneity and fixed degree skewness $\delta_z = 10$. Panel (a) corresponds to the classic Watts phase diagram of contagion, with $\sigma = 0$ and $\delta_1 = 1$. Panels (a-d) are identical in connectivity, with $\langle w \rangle = 1$ and edge weight progressively skewed. The standard deviations correspond to weight distributions of $\mathbf{w} = (1, 1)^T$, $(3.5, 0.74)^T$, $(6, 0.5)^T$ and $(8.6, 0.23)^T$, respectively. Heat-maps come from numerical simulations by averaging over 10^3 perturbations of a single infected node in a network of size $N = 10^5$. Dashed lines show solutions from linear stability analysis. Networks have no overlap ($\gamma = 0$) and no spontaneous adoption ($p = 0$).

To better understand the dynamics of our model, we first consider the case with non-zero rate of spontaneous adoption ($p > 0$) and explore the effects of varying edge weight heterogeneity and layer overlap. The former case can be studied by tuning the weight scaling factor δ_w , or equivalently, the weight standard deviation σ defined by $\sigma^2 = \sum_{i=1}^M P_i(w)(w_i - \langle w \rangle)^2$, where $P_i(w)$ is the probability that a randomly selected edge has weight w_i . Since weights are identical in a given layer, $P_i(w) = z_i/z$ (for further details see SI). In Erdős-Rényi (ER) networks or configuration model networks with scale-free (SF) degree

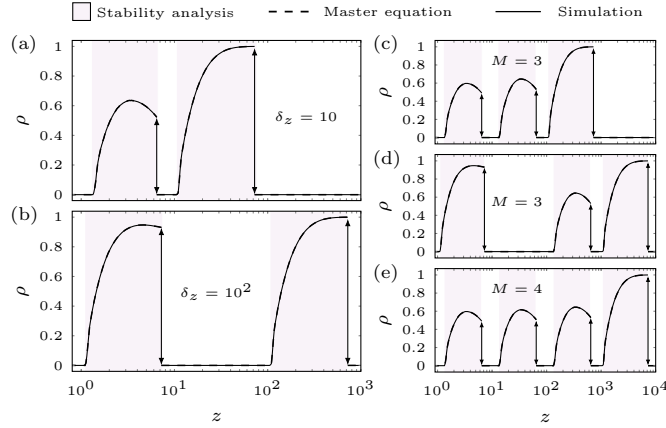


FIG. 4. Expected final cascade size $\rho(\infty)$ as a function of average degree z for constant threshold $\phi = 0.15$ and maximal weight heterogeneity ($\delta_w \ll 1$). (a, b) Increasing density skewness δ_z delays the onset of upper (higher z) phases of contagion, and allows larger cascades in lower phases in an $M = 2$ layer multiplex. (c-e) Increasing the number of layers to $M = 3$ and 4 induces 6 and 8 phase transitions in cascade size, respectively, for increasing z . (d) Nonlinear scaling of density skewness δ_z , such that $z_2/z_1 = 100$, and $z_3/z_2 = 10$. All results are averaged over 10^3 realizations of a $N = 10^7$ node multiplex, perturbed by a single infected node at $t = 0$. In all cases edge weights are maximally skewed, given that $w = 1$ and $w_i > 0$ for all layers i .

distributions, varying edge weight heterogeneity can accelerate or decelerate spreading (Fig. 2). We have studied this effect previously [14], showing that spreading speed is determined by competition between node configurations (\mathbf{k}, \mathbf{m}) whose adoption is either facilitated or hindered by a given weight distribution. To quantify the effects of layer overlap [43] on the dynamics, we consider the simplest case of $M = 2$ layers and introduce the overlap parameter $\gamma = |E_1 \cap E_2|/|E_1|$, where E_i is the edge set in layer $i = 1, 2$ ($|E_1| < |E_2|$). Via a similar mechanism as edge weight heterogeneity, layer overlap tends to speed up or slow down contagion (Fig. 2c-e). This occurs since a change in γ implicitly varies the weight distribution in the monoplex projection of the multiplex network, with weights being additive for overlapping edges. However, when weight heterogeneity is large, a composite edge is always dominated by the layer with the strongest weight, thus diminishing the effect of layer overlap. We also observe sudden deceleration in the diffusion of global cascades, evident as plateaus in $\rho(t)$, an effect due to weight heterogeneity discussed in [14] and further below. Results obtained via master equations and simulations are indistinguishable in all investigated measures (Fig. 2).

Single-layer threshold models of social contagion predict large-scale cascades of adoption for relatively sparse networks, with global cascades becoming exponentially rare once the network is sufficiently connected. In these models, system-wide contagion is only possible for a constrained area in (ϕ, z) -space with low values of ϕ and z , where susceptible nodes vulnerable to adoption due to a single infected neighbor form a percolating cluster [8, 10]. In multiplex networks with edge weight heterogeneity, however, nodes may be vulnerable to infected neighbors of one type, but not another, thus changing the conditions for contagion (Fig. 3). We demonstrate this effect by computing the expected final density of infected nodes $\rho(\infty)$ after introducing a single infected node ($p = 0$) in networks of $M = 2$ layers, with no link overlap ($\gamma = 0$) but with increasing weight heterogeneity controlled by σ . As σ increases [panels (a) to (d) in Fig. 3], previously stable nodes may become vulnerable to infection due to the emerging high-weight neighbors in the sparser layer, inducing cascades even in networks with large average degree z . This region is accurately predicted by linear stability analysis (dashed lines in Fig. 3) and by studying the velocity field $\dot{\nu}_j$ of Eq. (2) (see SI). In the presence of sufficient weight heterogeneity, (ϕ, z) -space allows for multiple and distinct phases of global cascades at constant ϕ , thus constituting a reentrant phase transition. In the low- z phase, cascades are mediated by the connectivity of the weak layer, since the strong layer is too sparse to allow a percolating cluster in that edge type. In the high- z phase, strong edges undergo percolation and determine the stability of adjacent nodes that would otherwise be stable due to the highly dense weak layer. These transitions are unchanged by link overlap, and are straightforward to observe with

other multiplex threshold rules (defined in Table I). Note that other threshold models can also generate additional transitions in (ϕ, z) space (for the multiplex *or* rule see SI, and for a model with assortativity see [34]).

By tuning the relative density parameter δ_z , or by introducing additional layers ($M > 2$), we observe global cascades at any scale of connectivity. We see that δ_z determines the average degree z at which global cascades are triggered (Fig. 4a and b). This is because the percolation transition of vulnerable nodes in the connectivity of individual layers allows the onset of subsequent cascading regions. Increasing the number of layers in the network creates additional phases of contagion (see Fig. 4c to e for $M = 3, 4$). When the relative density scales non linearly with the layers, the onset of contagion phases may be delayed or promoted (Fig. 4d). We observe that in multiplex networks exhibiting reentrant phases, strong edges that are too sparse to percolate structurally inhibit cascades driven by edges that are denser but weaker, leading to “partial” cascades that are global but do not fill the network (see rightmost peak of the lower phase in Fig. 3d and Fig. 4, and discussion in SI). This is due to the “immunizing” effect of strong edges in information diffusion. That is, pairs of susceptible nodes connected by a sufficiently strong edge are impossible to infect if all other neighbors are weak, even if all those weak neighbors are infected. These configurations are abundant when the strong layer is yet to undergo a structural percolation transition, accounting for the decrease in cascade size for increasing z within a single cascading phase.

DISCUSSION

Our results demonstrate that global information cascades are possible in systems that appear highly robust, that is, large networks with arbitrarily high connectivity. This is a consequence of nodes allocating finite resources to form edges of heterogeneous cost, in a way that maximizes the entropy of the resulting network. We conclude that if network connectivity is to provide resistance to global cascades, it must be via edges of sufficient homogeneity. We have interpreted node resources as total edge weight, conceptualizing the system as a multiplex whose layers vary by edge weight and density. As the consequence of a multiplex structure where layer density is inversely related to its weight, the phase transitions in cascade size are reentrant. In other words, growing networks pass through alternating phases of stability and instability to external shocks. We observe these phenomena in simulations, and confirm our results using a master equation formalism that we have extended to multiplex networks. This formalism allows a linear stability analysis, enabling us to calculate the phase boundary of the system. Due to the strong empirical support of intimacy circle theory, we expect the reentrant phase transitions predicted by our model to be validated by real-world data on contagion processes. Yet, we also expect that in real instances of complex contagion where weight distributions are quasi-continuous, the distinct regions we observe in the phase space become superimposed. Thus, although the phase space would no longer be discretized, edge-heterogeneity would continue to promote global cascades at high connectivity via similar mechanisms. Our results provide a novel and strikingly simple explanation for how information cascades may develop in highly dense, heterogeneous settings, and suggest approaches to network design that promote or suppress system-wide cascades of threshold driven contagion.

Acknowledgement

We acknowledge the Pôle Scientifique de Modélisation Numérique (namely L. Taulelle) from ENS Lyon for their computing support; D. Knipf for support in the initial stages of the project; and the ACADEMICS (IDEX-Lyon), SoSweet (ANR-15-CE38- 0011), and MOTif (18-STIC-07) projects.

SUPPLEMENTARY INFORMATION

ANALYTIC SOLUTION

Reduced dimension master equation

In this work we extend the edge-heterogeneous approximate master equation formalism, first presented in [14] and described in detail in the Supplementary Information of that text, to multiplex networks. This formalism is configuration based, meaning that we solve for the densities of susceptible nodes over time t according to their local configurations, denoted (\mathbf{k}, \mathbf{m}) . In the lowest level of its formulation, we solve a rate equation for all densities of each class $s_{\mathbf{k}, \mathbf{m}}$ and $i_{\mathbf{k}, \mathbf{m}}$, or the fraction of susceptible and infected nodes, respectively, with degree vector \mathbf{k} , that have partial degree vector \mathbf{m} at time t . We do not reproduce these rate equations here as they are described in detail in [14]. The functions $g_j(\nu, t)$ and $h(\nu, t)$ in the reduced master equation formalism are defined by

$$g_j(\nu, t) = f_t + (1 - f_t) \sum_{\mathbf{k}} \frac{k_j}{z_j} P(\mathbf{k}) \sum_{\mathbf{m}} f(\mathbf{k}, \mathbf{m}) B_{k_j-1, m_j}(\nu_j) \prod_{i \neq j} B_{k_i, m_i}(\nu_j) \quad (4)$$

and

$$h(\nu, t) = f_t + (1 - f_t) \sum_{\mathbf{k}} P(\mathbf{k}) \sum_{\mathbf{m}} f(\mathbf{k}, \mathbf{m}) \prod_{j=1}^n B_{k_i, m_i}(\nu_j), \quad (5)$$

with

$$f_t = 1 - (1 - p)e^{-pt}. \quad (6)$$

Here, $P(\mathbf{k})$ is the probability that a randomly selected node has degree vector \mathbf{k} . Given that our multiplex is maximally random up to the degree distribution of each edge type, and that the degrees of each type are uncorrelated, $P(\mathbf{k})$ can be expressed as the probability of a node having total degree k , comprised of layer degrees k_i summing to k . If p_{k_i} is the probability of a node having degree k_i in layer i , alternatively $P_i(k)$, we can write

$$P(\mathbf{k}) = P(k) P(k_1, \dots, k_n; k, p_{k_1}, \dots, p_{k_n}), \quad (7)$$

where the second term is the multinomial distribution. As such we have $\sum P(\mathbf{k}) = 1$. Further, f is the response function of the configuration (\mathbf{k}, \mathbf{m}) , defined as

$$f(\mathbf{k}, \mathbf{m}) = \begin{cases} 0 & q_{\mathbf{m}} < \phi q_{\mathbf{k}}, \\ 1 & q_{\mathbf{m}} \geq \phi q_{\mathbf{k}} \end{cases}, \quad k > 0, \quad (8)$$

with $q_{\mathbf{k}} = \mathbf{k} \cdot \mathbf{w}$ and $q_{\mathbf{m}} = \mathbf{m} \cdot \mathbf{w}$, whereas $B_{k_i, m_i}(\nu_j)$ is a binomial factor. Finally, the reduced dimension master equations can be written as

$$\dot{\nu}_j = g_j(\nu, t) - \nu_j, \quad (9a)$$

$$\dot{\rho} = h(\nu, t) - \rho. \quad (9b)$$

Cascade condition for $p = 0$

We may also use the AME formalism in the case $p = 0$ (no spontaneous infection) to derive a cascade condition, as has been done previously for the Watts model [49] and for the unweighted version of our

model [10]. First we observe that by assuming $p = 0$, $f_t = 0$ and thus we remove the explicit time dependence in Eqs. (4) and (5), i.e. $g_j = g_j(\boldsymbol{\nu})$ and $h = h(\boldsymbol{\nu})$. Then, by using the response function of 8, the sum over \mathbf{m} in $g_j(\boldsymbol{\nu})$ can be rewritten as

$$g_j(\boldsymbol{\nu}) = \sum_{\mathbf{k}} \frac{k_j}{z_j} P(\mathbf{k}) \sum_{\mathbf{m}} f(\mathbf{k}, \mathbf{m}) B_{k_j-1, m_j}(\nu_j) \prod_{i \neq j} B_{k_i, m_i}(\nu_i) \quad (10)$$

Then, we perform a linear stability analysis of the reduced AME system (9) around the fixed point $(\boldsymbol{\nu}^*, \rho^*) = (\mathbf{0}, 0)$, corresponding to a total lack of infection. If $(\boldsymbol{\nu}^*, \rho^*)$ is unstable, then any small perturbation (like a single infected node at $t = 0$) can drive the system out of equilibrium and create a global cascade of infection where $\rho > 0$, that is, a system where a non-vanishing fraction of nodes is infected in the limit $N \rightarrow \infty$. Since the system $\dot{\nu}_j = g_j(\boldsymbol{\nu}) - \nu_j$ is closed, the stability of 9 is determined by the stability of this equation at $\boldsymbol{\nu}^* = \mathbf{0}$. According to linear stability theory, a local instability exists if the Jacobian matrix of the system evaluated at the fixed point,

$$J_{ji}^* = -\delta_{ji} + \left. \frac{\partial g_j(\boldsymbol{\nu})}{\partial \nu_i} \right|_{\boldsymbol{\nu}=\boldsymbol{\nu}^*}, \quad (11)$$

has at least one eigenvalue with a real part larger than zero. We can write the partial derivative in 11 explicitly by considering the expansion of $B_{k_i, m_i}(\nu_j)$ in Eq. 4,

$$\frac{\partial g_j}{\partial \nu_i} = \begin{cases} \sum_{\mathbf{k}, \mathbf{m}} \frac{k_j}{z_j} P(\mathbf{k}) f(\mathbf{k}, \mathbf{m}) \dot{B}_{k_j-1, m_j}(\nu_j) \prod_{i \neq j} B_{k_i, m_i}(\nu_i) & j = i \\ \sum_{\mathbf{k}, \mathbf{m}} \frac{k_i}{z_j} P(\mathbf{k}) f(\mathbf{k}, \mathbf{m}) B_{k_j-1, m_j}(\nu_j) \dot{B}_{k_i, m_i}(\nu_i) \prod_{l \neq j, i} B_{k_l, m_l}(\nu_l) & j \neq i \end{cases} \quad (12)$$

where

$$\dot{B}_{k_j-1, m_j}(\nu_j) = \binom{k_j-1}{m_j} [m_j \nu_j^{m_j-1} (1-\nu_j)^{k_j-1-m_j} - (k_j-1-m_j) \nu_j^{m_j} (1-\nu_j)^{k_j-2-m_j}] \quad (13)$$

and $\dot{B}_{k_j, m_j}(\nu_i)$ is written similarly (by making the changes $j \rightarrow i$ and $k_j - 1 \rightarrow k_i$). Then, for $j = i$ we analyse terms in the sum over \mathbf{m} at the fixed point $\boldsymbol{\nu}^* = \mathbf{0}$: For $m_j = 0$ we have $\dot{B}_{k_j-1, 0}(0) = 1 - k_j$, but since $B_{k_i, m_i}(0) = \delta_{m_i, 0}$ and $f(\mathbf{k}, \mathbf{0}) = \mathbf{0}$ for $\phi > 0$, the associated term in 12 is zero. For $m_j = 1$ we have $\dot{B}_{k_j-1, 1}(0) = k_j - 1$. Finally, for $m_j > 1$ we get $\dot{B}_{k_j-1, m_j}(0) = 0$, so the only non-zero term corresponds to $m_j = 1$. By a similar argument, for $j \neq i$ the only surviving term in 12 is $\dot{B}_{k_i, 1}(0) = k_i$ (for $m_i = 1$).

Combining these results, we can write 11 explicitly as

$$J_{ji}^* = -\delta_{ji} + \sum_{\mathbf{k}} \frac{k_j}{z_j} (k_i - \delta_{ji}) P(\mathbf{k}) f(\mathbf{k}, \mathbf{e}_i), \quad (14)$$

where, as before, \mathbf{e}_i is the i -th basis vector of dimension n . The Jacobian matrix \mathbf{J}^* , whose elements are given by 14, contains the structure of the multiplex, namely the degree and weight distributions via $P(\mathbf{k})$, as well as node dynamics, via the response function $f(\mathbf{k}, \mathbf{e}_i)$, which provides the response of a node with degree vector \mathbf{k} to a single infected neighbour across an i -type edge. The eigenvalues λ_j of \mathbf{J}^* are obtained by solving the characteristic equation $\det |\mathbf{J}^* - \lambda \mathbf{1}| = 0$. Then, the cascade condition for our model (in the case $p = 0$) is

$$\text{Re}(\lambda_j) > 0 \quad (15)$$

for at least some $j = 1, \dots, n$. If we denote by $z = \sum_j z_j$ the average degree in the network, this condition defines the area in (ϕ, z) -space where global cascades of infection may develop, for a given weight distribution $P(\mathbf{w})$. Even though we cannot write an algebraic formula for λ_j when $n > 4$, we can compute the eigenvalues numerically. We may also find an explicit expression for the cascade condition in

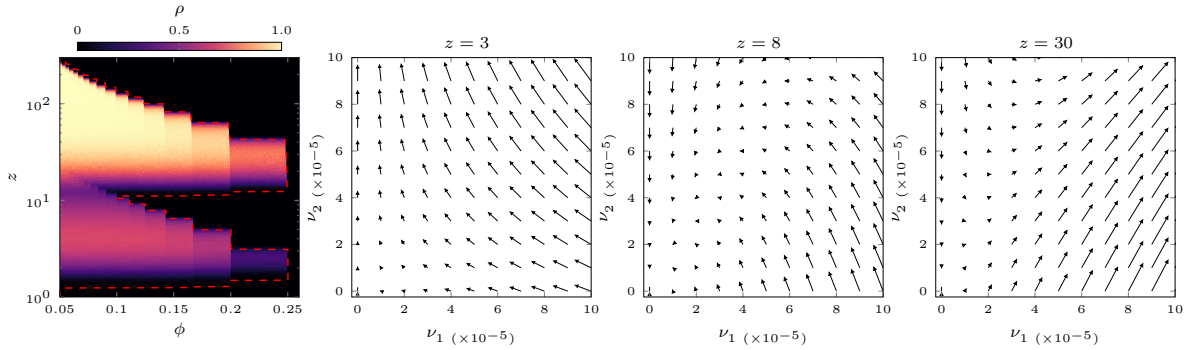


FIG. 5. Velocity fields around the fixed point $\nu = \mathbf{0}$, indicating the stability of the system at three points along the $\phi = 0.15$ axis, in the lower cascade window at $z = 3$, between cascade windows at $z = 8$, and in the upper cascade window, at $z = 30$. In the lower window, low weight links ($i = 2$) provide most of the connectivity, and allow the emergence of a percolating vulnerable cluster. Hence, the system is unstable in the ν_2 axis, while sparse, high weight links serve to inhibit the size of resultant cascades at these z scales. Between cascade windows at $z = 8$ the fixed point is a sink, since nodes are stable to low weight neighbour adoption, and high weight neighbours are too sparse to percolate structurally. At $z = 30$, nodes are mostly connected through low weight neighbours to whom they are stable, but sparse, high weight neighbours ($i = 1$) now percolate structurally, and dominate the strength of adjacent nodes. This forms a percolating vulnerable cluster, and the system is unstable along the ν_1 axis. Beyond this window, nodes are stable against adopting neighbours of all weights.

simple cases such as a bimodal weight distribution, as we will do in the following section.

Eigenvalues for $M = 2$ non-overlapping layers

The characteristic equation is $\lambda^2 - \lambda \text{Tr} \mathbf{J}^* + J_{11}^* J_{22}^* - J_{12}^* J_{21}^* = 0$, with solution given by

$$\lambda_{1,2} = \frac{1}{2} \left[\text{Tr} \mathbf{J}^* \pm \sqrt{(\text{Tr} \mathbf{J}^*)^2 - 4(J_{11}^* J_{22}^* - J_{12}^* J_{21}^*)} \right], \quad (16)$$

where $\text{Tr} \mathbf{J}^* = J_{11}^* + J_{22}^*$ is the trace of the Jacobian matrix. From 14 we have $J_{12}^*, J_{21}^* \geq 0$, so the eigenvalues in 16 are real numbers. Then, we may write the cascade condition of our model (for $p = 0$) in the case of a bimodal weight distribution as

$$\text{Tr} \mathbf{J}^* \pm \sqrt{(J_{11}^* - J_{22}^*)^2 + 4J_{12}^* J_{21}^*} > 0. \quad (17)$$

In the limit $\sigma \rightarrow 0$, 17 reduces to the cascade condition of the unweighted Watts model [10, 49]. Otherwise, 17 determines two (usually overlapping) regions in parameter space where global cascades may develop, depending on the sign of the square root (Fig. 5).

MULTIPLEX CONFIGURATION MODEL ALLOWING FOR EDGE SET OVERLAP

In order to implement an $M = 2$ layer multiplex with overlap using the configuration model, we require three projected edge types (see Fig. 1 in main text). Edge types $j = 1$ and 2 are non-overlapping projections of layer 1 and 2 edges respectively, whereas $j = 3$ type edges are composite edges formed by their overlap. The degree distribution is Erdős-Rényi, within layers as well as in overlapping edges. We denote the average degree of the three composite link types by c_1 , c_2 and c_3 , so that we have $z_1 = c_1 + c_3$, and $z_2 = c_2 + c_3$. Assuming total average degree $z = z_1 + z_2$, overlap γ and density scaling constant δ_z , it is straightforward to obtain the relations $c_1 = z_1(1 - \gamma)$, $c_2 = z_1(\delta_z - \gamma)$ and $c_3 = z_1\gamma$, where $z_1 = z/(1 + \delta_z)$.

MONTE CARLO SIMULATION OF BINARY-STATE DYNAMICS

We implement numerically a multiplex network using the multivariate configuration model, which entails $2^M - 1$ independent applications of the single layer configuration model, one for each composite link type. Since layer overlap is accounted for by the use of composite edges, we do not allow for double edges in the resultant network. Complex contagion is implemented numerically via Monte Carlo simulations of a monotone binary-state dynamics, where nodes are selected uniformly at random for update in asynchronous order, generating a series of time steps. Once a node state changes from susceptible to infected, it remains so for the rest of the dynamics, thus ensuring a steady state in a finite simulation. Each time step consists of N node updates, where a randomly selected node becomes spontaneously infected with probability p , and adopts otherwise only if the threshold rule is satisfied.

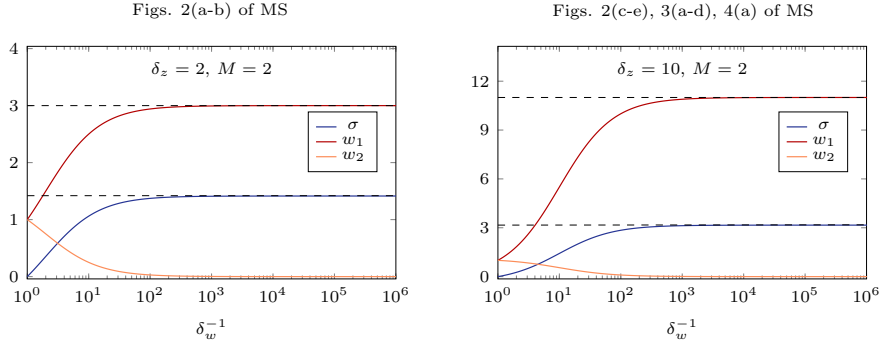


FIG. 6. Weight standard deviation σ and weight values \mathbf{w} for simulations in the main text (MS). In Figs. 2(a-b) of the main text, we simulate and solve analytically an $M = 2$ layer multiplex with degree skewness $\delta_z = 2$. We choose $\sigma = 0, 0.6$ and 1.2 , which corresponds to the degree vectors $\mathbf{w} = (1, 1)^T, (1.8, 0.6)^T$ and $(2.7, 1.5)^T$. Due to the constraints $w_i > 0$ for all i and $\langle w \rangle = 1$, σ tends to an upper limit of $\sigma_{\max} \simeq 1.41$. In Figs. 2(c-e) of the main text we set $\delta_z = 2$, again with $M = 2$, and choose $\sigma = 0, 2.5$ and 2.8 , corresponding to the degree vectors $\mathbf{w} = (1, 1)^T, (9, 0.2)^T$ and $(10, 0.1)^T$, respectively. As weight heterogeneity δ_w increases, the standard deviation tends towards $\sigma_{\max} = 3.16$. In this same network configuration in Figs. 3(a-d), we set $\sigma = 0, 0.8, 1.6$ and 2.4 , corresponding to weights of $\mathbf{w} = (1, 1)^T, (3.5, 0.74)^T, (6, 0.5)^T$ and $(8.6, 0.23)^T$.

DEGREE AND WEIGHT DISTRIBUTIONS

In our model, all edges in layer i of the multiplex have weight w_i . The mean weight $\langle w \rangle$ can therefore be found by summing over layers,

$$\langle w \rangle = \sum_{i=1}^M \frac{z_i}{z} w_i, \quad (18)$$

where z_i is the average degree of nodes in layer i , and z is the total average degree, $z = z_1 + \dots + z_M$. We constrain $\langle w \rangle = 1$ across all simulations in this work, as we are interested in studying the effect of varying the skewness δ_z in edge density, and the skewness δ_w in interaction strength, across layers. For simplicity, we assume that these quantities scale linearly for successive layers,

$$w_{i+1} = \delta_w w_i \quad \text{and} \quad z_{i+1} = \delta_z z_i, \quad (19)$$

where $\delta_z \geq 1$ and $\delta_w \leq 1$ indicate a multiplex growing in link density, and decreasing in interaction

strength or weight, by layer. The standard deviation of edge weights across the network is defined as

$$\sigma^2 = \sum_{i=1}^M P_i(w) (w_i - \langle w \rangle)^2, \quad (20)$$

where $P_i(w)$ is the probability that a randomly selected edge has weight w_i . In the simulations described in the main text, we first set a density skewness δ_z , and then increase weight skewness subject to the constraints that all weight values are positive ($w_i > 0$ for all layers i) and that $\langle w \rangle = 1$. These constraints induce an upper bound on the weight standard deviation σ , which we call σ_{\max} (Fig. 6).

PHASE SPACE FOR $M = 3$ LAYERS AND PARTIAL CASCADES

In Fig. 4(c) of the main text we show a $\phi = 0.15$ slice of an $M = 3$ layer multiplex, with weight standard deviation σ set to its maximum value of 10.5. Here in the SI we reproduce the entire phase space for this network (Fig. 7(a)). Partial cascades are evident in the first two regions of the phase space. As it has been first observed in [8], partial cascades are a subset of global cascades, which fill up a small (but still infinite) fraction of the underlying network, even in the infinite size limit ($N \rightarrow \infty$). Earlier it has been argued that their size is determined by the connected component of the network hosting the actual cascade, thus the size of the largest cascade is well approximated by the largest connected component of the network. However, as observed for example in Fig. 4(c) and Fig. 7(a), partial cascades emerge in weight heterogeneous multiplex networks even if the underlying network is connected in a single component, thus every node in the network are potentially available for the evolving cascade. This phenomena is due to the local “immunising” effects of stronger ties yet not forming a percolating sparse layer, as explained in the main text.

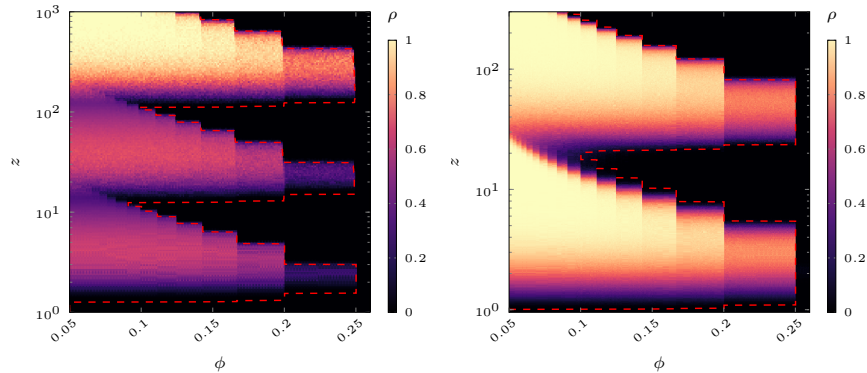


FIG. 7. Weighted multiplex rule with $M = 3$ (left) and the multiplex *or* rule with $M = 2$ (right). We plot the expected density $\rho(\infty)$ of steady state contagion after single node perturbation in an $M = 3$ layer network, with $\delta_z = 10$ and maximum edge weight heterogeneity ($\delta_w \ll 1$). Partial cascades are evident in the first two windows, with the entire network adopting only at very high levels of connectivity, when even the sparsest edge type has undergone structural percolation. In the multiplex *or* phase space, we set $\delta_z = 20$, and note that relative edge weight δ_w is irrelevant, since layers are considered separately.

ANALYTIC SOLUTION FOR A MULTIPLEX THRESHOLD RULE

The reduced AMEs in Fig. 2 of the main text require a step function activation rule over the space of all (\mathbf{k}, \mathbf{m}) classes in order to be valid. Although we have focused our attention on the weighted multiplex rule, the multiplex *and* and *or* rules appear as step functions in configuration space (Fig. 7). We observe

that stability analysis is in excellent agreement for the Watts phase space (ϕ, z) under the multiplex *or* rule. Results differ fundamentally to those of the weighted multiplex rule - each node update requires $M = 2$ applications of the threshold rule, and since layers are independent, they no longer interact and produce partial cascades, a distinctive feature of the weighted threshold rule.

-
- [1] J. Borge-Holthoefter, R. A. Baños, S. González-Bailón, and Y. Moreno, *J. Complex Netw.* **1**, 3 (2013).
- [2] E. M. Rogers, *Diffusion of innovations* (Simon and Schuster, 2010).
- [3] D. Centola and M. Macy, *Am. J. Sociol.* **113**, 702 (2007).
- [4] R. I. Dunbar, *J. Human Evolu.* **22**, 469 (1992).
- [5] B. Gonçalves, N. Perra, and A. Vespignani, *PloS ONE* **6**, e22656 (2011).
- [6] R. I. Joh, H. Wang, H. Weiss, and J. S. Weitz, *B. Math. Biol.* **71**, 845 (2009).
- [7] T. Takaguchi, N. Masuda, and P. Holme, *PloS One* **8**, e68629 (2013).
- [8] D. J. Watts, *Proc. Nat. Acad. Sci.* **99**, 5766 (2002).
- [9] M. Granovetter, *Am. J. Sociol.* **83**, 1420 (1978).
- [10] Z. Ruan, G. Iñiguez, M. Karsai, and J. Kertész, *Phys. Rev. Lett.* **115**, 218702 (2015).
- [11] P. D. Karampourniotis, S. Sreenivasan, B. K. Szymanski, and G. Korniss, *PloS One* **10**, e0143020 (2015).
- [12] R. I. Dunbar, *Philos. Trans. Royal Soc. B* **367**, 2192 (2012).
- [13] H.-H. Jo, Y. Murase, J. Török, J. Kertész, and K. Kaski, *Physica A* **500**, 23 (2018).
- [14] S. Unicomb, G. Iñiguez, and M. Karsai, *Sci. Rep.* **8**, 3094 (2018).
- [15] R. Burkholz, A. Garas, and F. Schweitzer, *Phys. Rev. E* **93**, 042313 (2016).
- [16] M. Karsai, G. Iñiguez, R. Kikas, K. Kaski, and J. Kertész, *Sci. Rep.* **6**, 27178 (2016).
- [17] E. Bakshy, J. M. Hofman, W. A. Mason, and D. J. Watts, in *ICWSM* (ACM, 2011) pp. 65–74.
- [18] J. Ugander, L. Backstrom, C. Marlow, and J. Kleinberg, *Proc. Nat. Acad. Sci.*, 201116502 (2012).
- [19] P. A. Dow, L. A. Adamic, and A. Friggeri, *ICWSM* **1**, 12 (2013).
- [20] J. P. Gleeson and R. Durrett, *Nat. Comm.* **8**, 1227 (2017).
- [21] M. S. Granovetter, in *Social networks* (Elsevier, 1977) pp. 347–367.
- [22] I. Kawachi and L. F. Berkman, *J. Urban Health* **78**, 458 (2001).
- [23] R. Dunbar, *Grooming, gossip, and the evolution of language* (Harvard University Press, 1998).
- [24] W.-X. Zhou, D. Sornette, R. A. Hill, and R. I. Dunbar, *Philos. Trans. Royal Soc. B* **272**, 439 (2005).
- [25] R. B. Cialdini and N. J. Goldstein, *Annu. Rev. Psychol.* **55**, 591 (2004).
- [26] J. C. Turner, *Social influence*. (Thomson Brooks/Cole Publishing Co, 1991).
- [27] M. Kivelä, A. Arenas, M. Barthelemy, J. P. Gleeson, Y. Moreno, and M. A. Porter, *J. Complex Networks* **2**, 203 (2014).
- [28] S. Boccaletti, G. Bianconi, R. Criado, C. I. Del Genio, J. Gómez-Gardenes, M. Romance, I. Sendina-Nadal, Z. Wang, and M. Zanin, *Phys. Rep.* **544**, 1 (2014).
- [29] K. Bruce, *Soc. Netw. Urban Situations* (1969).
- [30] L. M. Verbrugge, *Social Forces* **57**, 1286 (1979).
- [31] O. Yağan and V. Gligor, *Phys. Rev. E* **86**, 036103 (2012).
- [32] C. D. Brummitt, K.-M. Lee, and K.-I. Goh, *Phys. Rev. E* **85**, 045102 (2012).
- [33] K.-M. Lee, C. D. Brummitt, and K.-I. Goh, *Phys. Rev. E* **90**, 062816 (2014).
- [34] Y. Zhuang, A. Arenas, and O. Yağan, *Phys. Rev. E* **95**, 012312 (2017).
- [35] R. I. Dunbar, *Behav. Brain Sci.* **16**, 681 (1993).
- [36] R. I. Dunbar, *Evolutionary Anthropology: Issues, News, and Reviews: Issues, News, and Reviews* **6**, 178 (1998).
- [37] P. V. Marsden and K. E. Campbell, *Social Forces* **63**, 482 (1984).
- [38] J.-P. Onnela, J. Saramäki, J. Hyvönen, G. Szabó, D. Lazer, K. Kaski, J. Kertész, and A.-L. Barabási, *Proc. Nat. Acad. Sci.* **104**, 7332 (2007).
- [39] I. Tamarit, J. A. Cuesta, R. I. Dunbar, and A. Sánchez, *Proc. Nat. Acad. Sci.* **115**, 8316 (2018).
- [40] M. Elliott, B. Golub, and M. O. Jackson, *Am. Econ. Rev.* **104**, 3115 (2014).
- [41] S. Battiston, D. Delli Gatti, M. Gallegati, B. C. Greenwald, and J. E. Stiglitz, *J. Econom. Dynamics and Control* **36**, 1121 (2012).
- [42] H. Amini, R. Cont, and A. Minca, *Math. Finance* **26**, 329 (2016).
- [43] D. Cellai, E. López, J. Zhou, J. P. Gleeson, and G. Bianconi, *Phys. Rev. E* **88**, 052811 (2013).
- [44] W. Gerstner, W. M. Kistler, R. Naud, and L. Paninski, *Neuronal dynamics: From single neurons to networks and models of cognition* (Cambridge University Press, 2014).

- [45] R. Iyer, V. Menon, M. Buice, C. Koch, and S. Mihalas, *PLoS Comput. Biol.* **9**, e1003248 (2013).
- [46] M. Karsai, G. Iníguez, K. Kaski, and J. Kertész, *J. Roy. Soc. Interface* **11**, 20140694 (2014).
- [47] J. P. Gleeson, *Phys. Rev. Lett.* **107**, 068701 (2011).
- [48] J. P. Gleeson, *Phys. Rev. X* **3**, 021004 (2013).
- [49] M. A. Porter and J. P. Gleeson, *Frontiers in Applied Dynamical Systems: Reviews and Tutorials* **4** (2016).